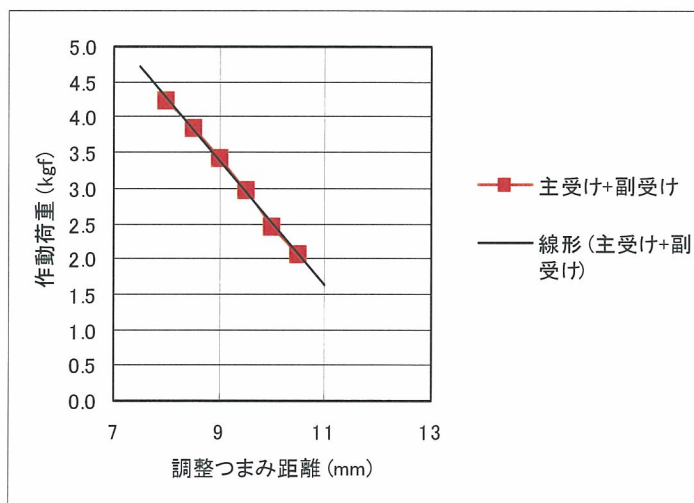粘性生体計測用機械荷重システムによる Sin 波の出力グラフ

メカニカルフューズの調整つまみと作動荷重の関係

Ⅲ．研究成果の刊行に関する一覧表

別紙4

研究成果の刊行に関する一覧表レイアウト（参考）

書籍

著者氏名	論文タイトル名	書籍全体の編集者名	書　籍　名	出版社名	出版地	出版年	ページ

雑誌

発表者氏名	論文タイトル名	発表誌名	巻号	ページ	出版年
Matsuyama J. Ohnishi I. Sakai R. Suzuki H. Harada A. Bessho M. Matsumoto T. Nakamura K.	A New Method for Measurement of Bone Deformation by Echo Tracking	Medical Engineering & Physics	28 (6)	588-95	2006
Kazuhiro Imai, Isao Ohnishi, Masahiko Bessho, Kozo Nakamura.	Nonlinear Finite Element Model Predicts Vertebral Bone Strength and Fracture Site.	Spine	31 (16)	1789-94	2006

Ⅲ．研究成果の刊行物・別刷

Technical note

A new method for measurement of bone deformation by echo tracking

J. Matsuyama[a], I. Ohnishi[a,*], R. Sakai[b], H. Suzuki[b], A. Harada[b], M. Bessho[a],
T. Matsumoto[a], K. Nakamura[a]

[a] *Department of Orthopaedic Surgery, University of Tokyo, 7-3-1 Hongo, Bunkyo-ku Tokyo 113-0033, Japan*
[b] *Research Laboratory, Aloka Co. Ltd., Tokyo, Japan*

Abstract

No method has been available to noninvasively detect bone deformation or strain under loading in vivo. We focused on ultrasonic measurement of the displacement at a certain point on a bone using the echo-tracking method (ET). To develop a method that can noninvasively detect bone deformation in vivo, a preliminary investigation was performed.

We investigated the accuracy of measuring displacement with our echo tracking system by using a flat metal panel and found that the method could measure displacement with a precision of a few microns.

A three-point bending test of a porcine tibia with both ends fully constrained was performed to measure bone surface displacement, and simultaneous measurement of the surface strain was done using two strain gauges. The correlation between the displacement measured by ET and the strain gauge readings was completely linear ($r = 0.999$), showing that the method could precisely detect bone deformation. The loads versus displacement curves obtained with cyclic loading were typical hysteresis loops that showed viscoelastic properties of the measured bone.

We also improved a multi-ET system capable of simultaneously tracking multiple points to detect deformation of the bone surface. Measurement by this echo tracking system was also compared with strain gauge readings during a three point bending test with both ends of the tibia supported. The linearity of both methods was very high ($r = 0.998$). Our ET method might have considerable potential for noninvasive measurement of bone viscoelasticity and plasticity.
© 2005 IPEM. Published by Elsevier Ltd. All rights reserved.

Keywords: Echo tracking; Bone deformation; Noninvasive measurement; Bone strain

1. Introduction

Bone is a self-repairing structural material that adapts its mass, shape, and properties to changes in mechanical requirements and tolerates voluntary physical activity throughout life without breaking or causing pain. Quantifying the mechanical inputs into bone is important for understanding the form and function of the skeleton. The forces applied to each bone at the organ level must be translated to the cellular level and then somehow play a role in the maintenance and adaptation of bone tissue [1–3].

Bone fails if subjected to a force exceeding its strength, but even physiological loading during daily activities causes deformation depending on a bone's mechanical properties. Determining the extent of which deformation normally occurs should help to elucidate the mechanotransduction mechanism in bone [4]. Therefore, it is important to be able to quantitatively measure the extent of bone deformation or strain under loading.

To date, many methods have been tried to detect bone deformation under a load [5,6]. A strain gauge is a device that measures the deformation of materials to which it is attached, and this has been the method used to quantify bone strains in vivo. The strain gauge is thus the gold standard for measuring bone deformation in vivo and this device has provided much useful data [7,8]. However, measurement with strain gauges requires invasive exposure of a site for attachment to the bone surface. To date, no method has been available to noninvasively detect bone deformation or strain under loading.

* Corresponding author. Tel.: +81 3 5800 8656; fax: +81 3 3818 4082.
  E-mail address: OHNISHII-DIS@h.u-tokyo.ac.jp (I. Ohnishi).

To overcome the above-mentioned limitations in the measurement of bone deformation, we focused on the use of ultrasound because of its noninvasiveness. Ultrasonic waves can penetrate soft tissues and visualize the bone surface. In addition, precise measurement of the displacement of a specific point can be achieved by the echo-tracking method. The echo tracking method measures extent of the displacement by tracking the initialized phase pattern of the radio frequency (RF) echo signal. Hokanson et al. [9] have developed an ultrasonic echo-tracking device that allows arterial wall motion to be measured transcutaneously using the standard pulse reflection technique. The motion of the echoes from the arterial wall was tracked by a gated threshold detector and converted into an analog output suitable for recording. The echo tracking method currently used for measuring arterial wall motion has an accuracy of one sixteenth of a wavelength which is an accuracy of 13 μm at every 1 mm/s with a 7.5 MHz probe [10].

Utilizing such an echo tracking method, it is possible to accurately and dynamically detect the displacement of a specific point on the surface of a bone. By detecting the displacement of multiple points on the bone surface under dynamic loading, it may be possible to detect dynamic bone deformation. The final goal of our investigations is to develop a method that can noninvasively detect bone deformation under loading in vivo by ultrasonic echo tracking method. For this purpose, a preliminary study was performed to confirm that our method had sufficient precision to detect bone surface deformation by conducting in vitro three-point bending tests of bone specimens.

2. Materials and methods

2.1. Echo tracking method

The accuracy of measuring the distance from a probe based on B-mode images depends on the ultrasound wave length and is the order of about 210 μm at a frequency of 7.5 MHz. In contrast, the echo tracking method is a technique measuring minute displacement of a certain point on a tissue with superior accuracy to standard ultrasound by detecting a wave
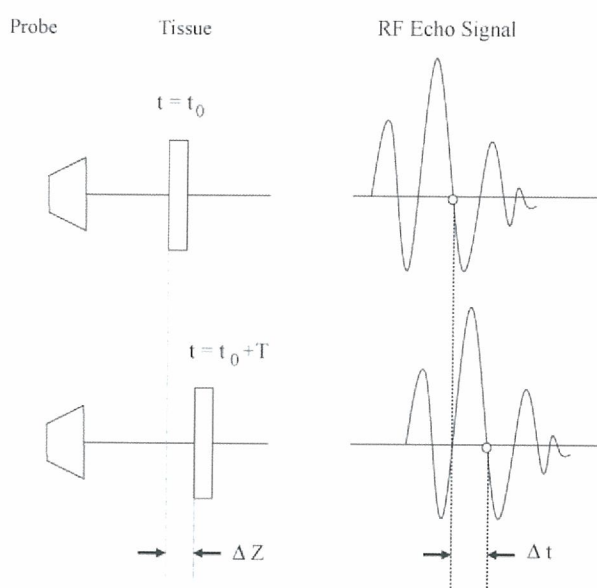

Fig. 1. A diagram of the principal of echo tracking method. Tissue at a certain depth is displaced at time ($t = t_0$) so that it moves away from the probe for a minute distance, ΔZ, during a single cycle of an ultrasonic wave pulse, T. This causes phase delay of a RF echo signal from a tissue for a very short period of time, Δt.

pattern in a RF echo signal reflected from the tissue. For example, it is assumed that a tissue at a certain depth is displaced at time ($t = t_0$), so that it moves away from a probe for a small distance of ΔZ during a single cycle period of an ultrasonic wave pulse, T. This causes phase delay of the RF echo signal from the tissue for a very small period of time, Δt (Fig. 1). The echo tracking method measures extent of the displacement by tracking the initialized phase pattern of the RF echo signal.

We developed the echo tracking system and originally designed the software to utilize the characteristics of the acoustic impedance of bone to accurately measure the displacement on the surface of a bone. A diagram of the echo tracking system specifically designed for bone was shown in Fig. 2. Ultrasound wave was transmitted to the bone surface with a 7.5 MHz linear probe connected to an ultrasonic diagnostic device (SSD-1000, Aloka, Tokyo, Japan). The RF
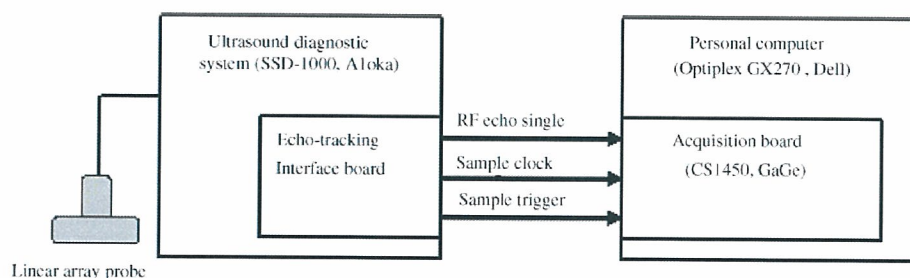

Fig. 2. A block diagram illustrating bone deformation measurement by echo tracking. The RF echo signal is recorded on a personal computer via the echo-tracking interface installed in the ultrasonography device. At the same time, a sample clock signal and sample trigger signal are transmitted to the PC synchronized with a transmit pulse repetition signal.

echo signal reflected from the bone surface was recorded on a personal computer (PC) (Optiplex GX270, Dell, TX, USA) via the echo-tracking interface installed in the ultrasonic diagnostic device. At the same time, a sample clock signal with a frequency of 50 MHz and a sample trigger signal with a frequency of 500 Hz were transmitted to the PC synchronized with a transmitting pulse repetition signal. The analog RF echo signal was converted into a 14-bit digital signal with a sampling frequency of 50 MHz by using a logging board (CS1450, GaGe, Montreal, Canada) installed in the PC and then the data were recorded. The stored RF echo data were interpolated to eight times to allow the detection of phase change with an equivalent sampling frequency of 400 MHz. These interpolated data were processed using software (LabVIEW, National Instruments, TX, USA) and the distance from the probe to each point on the bone surface was calculated.

2.2. Accuracy assessment of the echo tracking method using an aluminum panel

With this echo tracking system, we first verified the accuracy of the displacement measured in vitro by an echo tracking system that has been newly developed for measurement of bone deformation. A flat panel of aluminum alloy (65 mm × 85 mm × 10 mm) was fixed to a stepping motor (PK566-A: Oriental motor Co. Ltd., Tokyo, Japan) via a columnar support (TSL120: Nippon Thompson Co. Ltd., Tokyo, Japan) with its surface vertical to the driving axis. To direct ultrasound vertically toward the center of the panel, a 7.5 MHz linear electronic echo probe (UST-5710-7.5: Aloka Co. Ltd., Tokyo, Japan) was fixed to a custom-made probe stand (Aloka Co. Ltd., Tokyo, Japan). The echo probe and the aluminum panel were mounted independently from each other and the distance between them was set at 10 mm in the water bath. The panel was immersed in a plastic water tank (538 mm × 680 mm × 400 mm) and was translated distally along the direction of the echo beam at a displacement rate of 500 μm/s using the stepping motor. The displacement of a central point of the panel surface was measured by the echo tracking system. The displacement of the panel was also measured simultaneously by a linear potentiometer (AT-104: Keyence Corporation, Osaka, Japan) with a proven accuracy of 1 μm at the flat surface of the columnar support above the water (Fig. 3A and B). The accuracy of the echo tracking system was evaluated by comparing these two measurements and the standard deviation (S.D.) of the difference between the displacement measured by the echo tracking and by the potentiometer was calculated. The data-sampling rate for the echo tracking system was 500 Hz and that for the potentiometer was 100 Hz. Throughout the experiment, the water temperature was kept at 24 °C.

2.3. A three point bending test using a porcine tibia with both ends fully constrained

To evaluate how accurately the echo tracking system detect bone deformation under loading by monitoring displacement
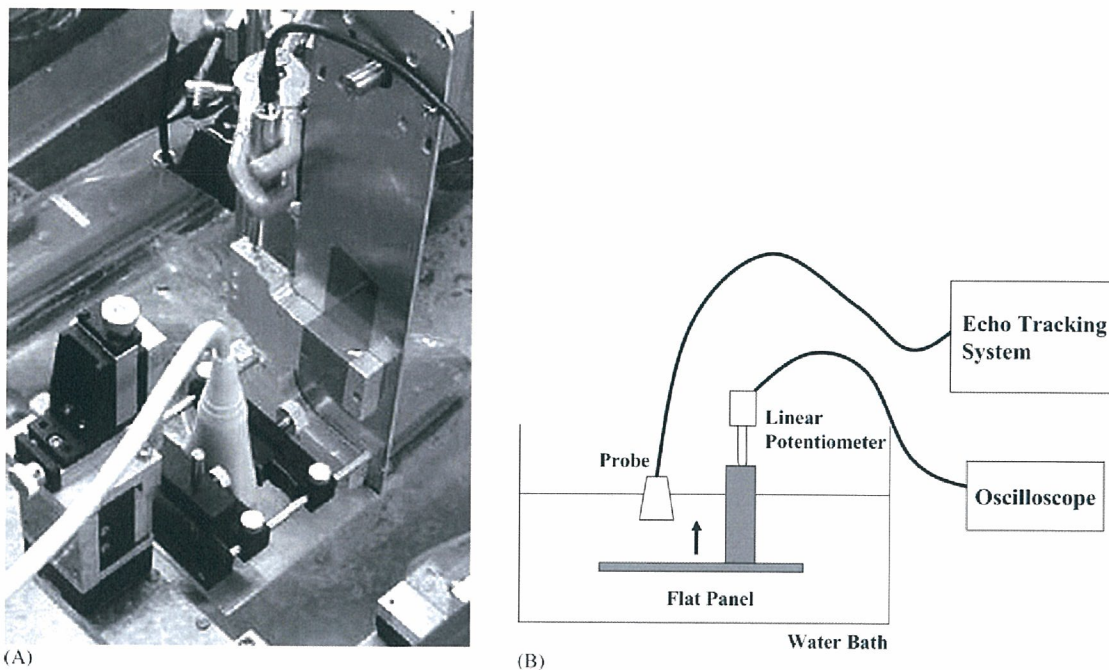

Fig. 3. (A and B) A flat panel fixed to a stepping motor via a columnar support in a plastic water tank vertically moved towards a 7.5 MHz linear electronic echo probe at a displacement rate of 500 μm/s. The displacement of a central point on the panel surface was measured by the echo-tracking system. The displacement of the panel was also measured simultaneously by a linear potentiometer.
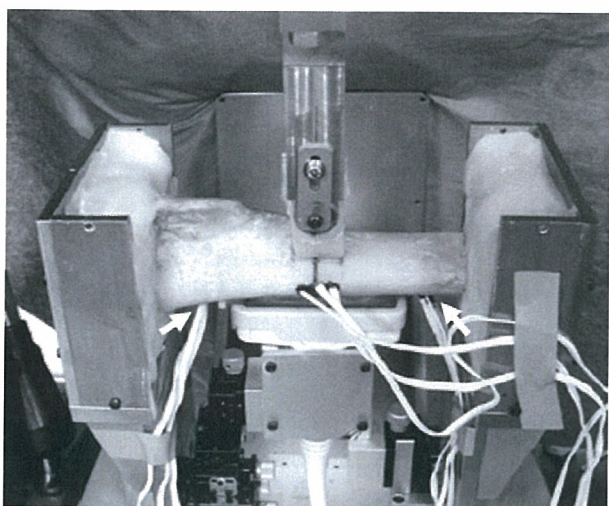
Fig. 4. After removing the soft tissues, the tibia was placed with its medial aspect upwards and both ends of the tibia were fully constrained with dental resin with a span of 214 mm. Two strain gauges were attached to the posterior aspect of the tibia at 50 mm proximal and 50 mm distal from the center of the tibia respectively. Displacement of the osseous surface was measured with the 7.5 MHz linear probe throughout the loading process and strain at each of the gauge sites was simultaneously measured. A single-cycle load and a three-cycle load were applied. (The white arrow on the left indicates the location of proximal strain gauge attached to the posterior bone surface and the white arrow on the right indicates the distal strain gauge.)

of the point on the bone surface, a three-point bending test using a porcine tibia was also performed to measure displacement at the surface of the tibia with the same echo tracking system. An adult porcine tibia with a length of 260 mm (preserved freshly frozen) was used for this experiment. After removing the soft tissues, the tibia was placed horizontally on a testing machine (Tensilon UTM-2.5T: A&D Co. Ltd., Tokyo, Japan) with its medial aspect upwards and both ends of the bone were fully constrained by dental resin (GC Ostron2®: GC, Tokyo, Japan) with a span of 214 mm. Two rosette strain gauges (KGF-1: Kyowa Electronic Instruments, Tokyo, Japan) were attached to the posterior aspect of the tibia at 50 mm proximal and 50 mm distal from center of the bone respectively. The displacement at the center of the bone surface was measured with the same probe throughout the loading process and the maximum principal strain at each of the gauge sites was measured simultaneously. A single-cycle load and a three cycle-load from 0 to 5780 N were applied at the center of the span of 214 mm in the lateral-medial plane using a resin pusher with a thickness of 25 mm and an actuator speed of 0.1 mm/s over a distance of 0.7 mm (Fig. 4). The sampling rate for the echo tracking system was 500 Hz and that for the strain gauges was 100 Hz. The room temperature was kept at 22 °C and the tibia was kept moistened with physiological saline throughout the experiment. The maximum principal strain measured by the two strain gauges was compared with the displacement shown by the echo tracking system.

2.4. A multi-echo tracking system

We also developed another echo tracking system (multi-echo tracking system) that was capable of simultaneously tracking multiple points. Five points were set along the long axis of the probe at intervals of 10 mm. Displacement at each of the five points was measured simultaneously, and surface deformation of the bone was shown as a third order spline complement curve defined by the displacement at the five points measured by the echo tracking system. The echo tracking system strain (ETS) was calculated by the following equation as a parameter of surface deformation.

$$ETS = D/L \qquad (1)$$

where L is the distance from the first tracking point to the fifth point, and D is the maximum distance from the spline curve to a straight line connecting the first and fifth tracking points. With this multi-echo tracking system, it is assumed that the displacement caused by translation to the direction of the echo beam and rotation in the plane including a loading point and five tracked points, is cancelled.

2.5. A three point bending test with proximal and distal metaphyses supported

To prove the multi-echo tracking system could detect bone deformation even when the measured object underwent some translation, we also measured the deformation of a porcine tibia. After the soft tissues were removed, the tibia with a length of 230 mm was placed horizontally on the testing machine (Servo Pulser, Shimadzu Corporation, Tokyo, Japan) with its medial aspect upwards and both sides of the metaphyses were supported by rollers with a span of 115 mm. A three-point bending load was applied by a resin pusher with a width of 25 mm at the mid point between the two supporting rollers (Fig. 5). Deformation and strain on the posterior surface of the tibia were measured simultaneously with a 7.5 MHz linear probe and two strain gauges (KGF-1, Kyowa, Tokyo, Japan). Five tracking points were set along the long axis of the tibia with the third point corresponding to the site of loading. The echo probe was fixed parallel to the posterior surface of the tibia at a distance of 20 mm. Two strain gauges were attached along the tracking line (a straight line formed by the five tracking points) at 5 mm distal and 5 mm proximal to the third point (center point) and with each gauge axis parallel to the tracking line. The gauge surfaces were waterproofed by coating tar (The Yokohama Rubber Company, Tokyo, Japan). Incremental load increases were applied from a preload of 100 N up to 1500 N. The loading rate was set at 25 N/s. Under each load, the ETS value and the readings of the two strain gauges set parallel to the tracking line were determined. The data sampling rate for echo tracking was 100 Hz and that for the strain gauges was 100 Hz. The correlation between the ETS value and each of the strain gauge readings was calculated with Pearson's cor-
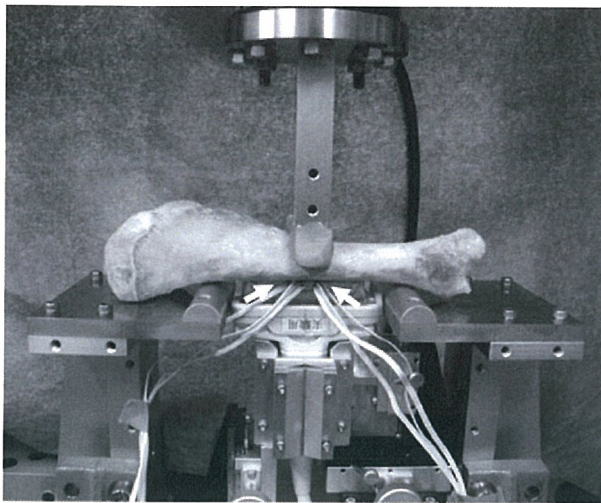
Fig. 5. The extracted porcine tibia was placed horizontally on the testing machine with a medial aspect upwards and both sides of the metaphysis were supported by rollers. Three-point bending loads were applied by a resin pusher from a preload of 100 N up to 1500 N. Deformation and strain of the posterior surface of the tibia were simultaneously measured with a 7.5 MHz linear probe and two strain gauges. Two strain gauges were attached to the tracking line at 5 mm distal and 5 mm proximal to the third tracking point with each gauge axis parallel to the tracking line. The gauge surfaces were waterproofed by coating tar. (The white arrow on the left indicates the location of proximal strain gauge attached to the posterior bone surface and the white arrow on the right indicates the distal strain gauge.)
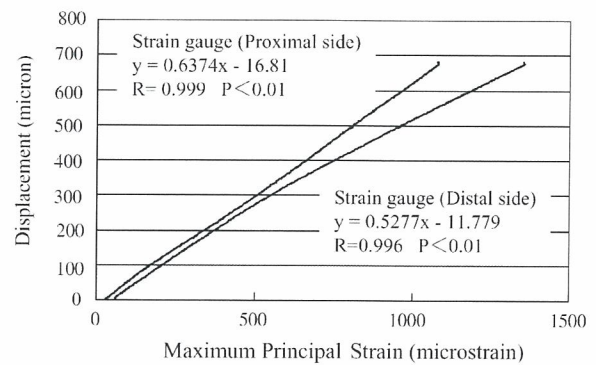

Fig. 6. Result of the single-cycle load in the three-point bending test of the porcine tibia. The graph showed that the strain gauge readings and those with the echo tracking system had an excellent linearity with a correlation coefficient of 0.999 and 0.996 all through the loading cycles.
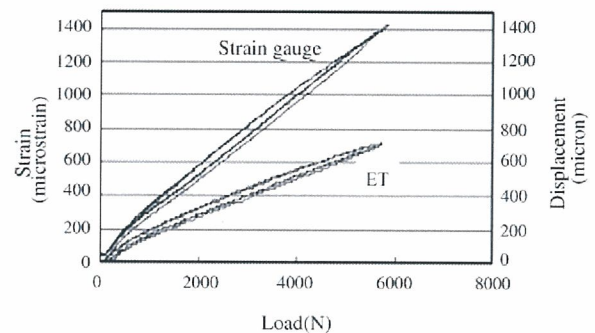

Fig. 7. Result of the three-cycle load in the three-point bending test of the porcine tibia. The curve relating the load magnitude with the data obtained from the strain gauge of the distal side was a typical hysteresis loop, indicating that the measured object was a viscoelastic material. The curve for the relationship between the load magnitude and the displacement of the echo tracking system was also a hysteresis loop.

relation analysis. The room temperature was kept at 22 °C and the tibia was kept moistened with physiological saline throughout the experiment. The sound speed used for the echo tracking measurement was set from the temperature of water in a bath and a bag attached to the probe according to the equation for the relation between water temperature and sound speed proposed by Greenspan [11].

3. Results

For measurement of the displacement of the flat panel, there was excellent linearity between the data obtained by the echo tracking system and the linear potentiometer ($r = 0.999$). The standard deviation (S.D.) of the difference between the displacement measured by the echo tracking system and that measured by the potentiometer was ±2.6 μm.

In the three-point bending test of the porcine tibia, the maximum principal strain recorded by the strain gauge set at 50 mm proximal to the loading point under a load of 5780 N (the maximum load) was 1077 micro strain and that at 50 mm distal was 1350 micro strain, whereas the displacement measured by echo tracking was 678.5 μm. The strain gauge readings and those of the echo tracking system showed excellent linearity with a correlation coefficient of 0.999 for the proximal strain gauge and 0.996 for the distal gauge (Fig. 6). The curve relating the load magnitude with the data obtained from each strain gauge was a typical hysteresis loop, indicat-

ing the measured bone was a visco elastic material. The curve for the relationship between the load magnitude and the displacement of the echo tracking system was also a hysteresis loop (Fig. 7).

In the study with the multi-echo tracking system, the strain readings of each gauge and the data from the entire system showed a perfect linear increase with the load. There was a linear relation between echo tracking data and each of the strain gauges ($r = 0.998$ and 0.998, respectively) (Fig. 8A and B). The reading for the gauge axis parallel to the tracking line and the maximum principal strain on the distal gauge at 1500 N was 1154.6 and 1160.4 micro strain, respectively. The angle of the direction of the maximum principal strain was 7° with reference to the echo tracking line.

4. Discussion

Bone shows deformation in response to an applied load. By quantitatively measuring this deformation, it is possible to assess the mechanical properties of bone material. Because
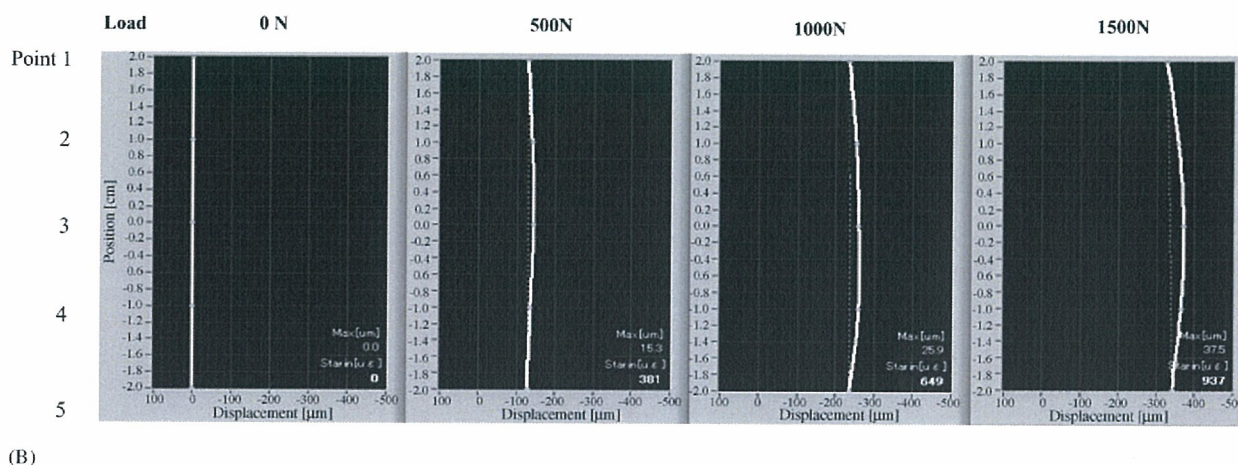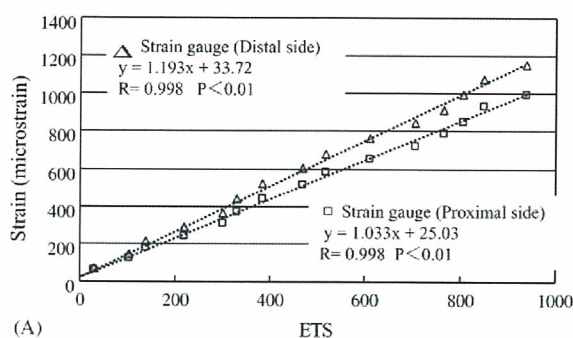
Fig. 8. (A) Result of the three-point bending test of the porcine tibia with the multi-echo tracking system. The strain readings of each gauge and the data from the entire system showed a perfect linear increase with the load. There was a linear relation between echo tracking data and each of the strain gauges ($r = 0.998$ and 0.998, respectively). (B) Result of the displacements at the five tracked points under the loads of 0, 500, 1000 and 1500 N. The surface deformation was visualized by a third order spline complement curve. The surface deformation increased with the increase of the load.

bone is a viscoelastic material, we can estimate its strength by measuring the elasticity, viscosity, and plasticity under dynamic loading. In this study, we attempted to develop an echo tracking method to noninvasively detect bone deformation under a load.

Numerous quantitative measurement methods using ultrasound have been tested to evaluate the elastic properties of bone or the fracture risk [12]. The axial transmission technique was based on the propagation of guided ultrasound waves along the bone surface. A set of ultrasound transducers (transmitters and receivers) was placed on the skin along the bone to measure the velocity of ultrasound waves passing through the cortical layer of the bone parallel to its axis. Sievanen et al. [13] reported in their study of the axial transmission technique that the cortical density was the only determinant of speed of sound measured in the radial and tibial shafts in vivo. The technique of measuring broadband ultrasound attenuation (BUA) and sound of speed (SOS) for the calcaneus was recently developed. Ultrasound transmitted to the calcaneus penetrates the bone and is detected by the receiver located on the opposite side. Then the stiffness of the bone is calculated from the measured BUA and SOS values. This stiffness index is reported to be closely correlated with

the regional bone mineral density measured by dual energy X-ray absorptiometry (DXA) [14]. These methods of quantitative evaluation by ultrasound technology have been based on measurement of the speed, permeability, and attenuation of ultrasound transmitted through the bone. In this respect, the echo tracking method that measures bone deformation differs markedly from these preceding ultrasound techniques.

Ultrasonography can clearly visualize the bone surface because the acoustic impedance of osseous tissue differs greatly from that of the surrounding soft tissues. However, the spatial resolution of B-mode images is not better than $100\,\mu m$. Therefore, measurement of bone deformation from B mode images is thought to lack sufficient precision, because resolution of better than $10\,\mu m$ is considered to be necessary to detect deformation compatible to that measured by a strain gauge, which can detect deformation of $0.001\,\mu m$ when the gauge length is 1 mm (the smallest available gauge). Thus, much more accurate measurement technology has been needed. Measurement of bone surface displacement using the echo tracking fulfils this requirement. The echo tracking method currently used for measuring arterial wall motion has an accuracy of one-sixteenth of a wave length, which is an accuracy of $13\,\mu m$ at every 1 mm/s with a 7.5 Hz probe. The

system was further improved to measure minute displacement of the bone and a much better precision of 2.6 μm could be obtained by improving the software to utilize the characteristics of the acoustic impedance of bone, so that minute displacement of tracked points on the bone surface could be measured.

The purpose of the first three-point bending test in which both ends were fully constrained was to evaluate whether the echo tracking system could in fact detect bone deformation accurately because the surface of bone was not flat and there was a possibility of the surface morphology changing when deformed. The accuracy of the system was assessed by directly comparing the data from our echo tracking method with those simultaneously recorded by the strain gauges. In this experiment, bone deformation should be regulated to occur in the direction of the echo beam. Because the probe was mounted firmly by an external support and faced the direction of loading, the echo tracking system could only detect displacement in the beam direction. The system used in this experiment could only detect displacement of a single point, so translation of the measured object should have been avoided. From the result of the experiment, we could prove that the correlation between the strain-related data from the echo tracking and the strain gauge readings was excellent. Therefore, the echo tracking method provided sufficient accuracy for detection of bone surface deformation.

Under a cyclic load, the system was able to monitor bone viscoelasticity because the load versus displacement curve was a hysteresis loop. It is well known that bone shows vicsoelasticity, but its nature has not been sufficiently investigated in vivo, because few techniques have been available to assess bone viscoelasticity in vivo. Only Moorcroft et al. [15] and Ohnishi et al. [16] have already investigated viscoelasticity in vivo using an external fixation system. To date, no method has been available to noninvasively assess the viscoelasticity of bone in vivo. However, it is very useful to assess bone viscoelasticity because it varies markedly during the process of fracture healing. The hysteresis loop shown by the echo tracking method indicated that it could be used to quantitatively assess in vivo viscoelasticity noninvasively in the future. Further investigations using bone models of known viscoelasticity will be needed to confirm the precision of the echo tracking system.

The purpose of the second three-point bending test in which both sides of the metaphyses were supported by rollers was to prove that the echo tracking system could detect bone deformation even when the measured object underwent some translation. Measurement of only one point is inadequate for detecting deformation because the displacement caused by translation of a moving object will be mixed. Accordingly, measurement of multiple points should be necessary to cancel the displacement caused by translation. Using the system with the multiple tracked points set along the straight line, it is assumed that the displacement caused by translation to the direction of the echo beam and rotation in the plane including the loading point and the five tracked points is cancelled.

The test in which both metaphyses were simply supported by rollers allows the tibia to translate to the direction of loading and to rotate within the frontal plane (the plane that includes the loading point and both supporting points). The magnitude of the strain measured by the strain gauges was an average strain of 1 mm gauge length, while the ETS measured an average strain of 40 mm. However, the linearity of both methods was very strong, indicating that only deformation components from the displacement data of five tracked points could be extracted even when the measured object underwent some translation. The strain along the tracking line was very close to the maximum principal strain and the difference in the direction of both was very small (only 7°). This indicated that the direction of strain at the center of the posterior surface of the tibia generated by three-point bending was almost parallel to that of the echo tracking line. By echo tracking measurement of multiple points, it is possible to optimize the detection environment depending on the pattern or mode of bone deformation under specific mechanical conditions by changing the interval and number of the measured points.

Our method has the technical limitation of only detecting deformation in the plane that includes the measured points because the tracking points were all located on a straight line. When bone deformation occurs in multiple planes, only the component of deformation in the measured plane can be detected, and the other components cannot be measured with the current system. To overcome this limitation, a measurement system should be developed with a three-dimensional distribution of multiple tracking points that is capable of detecting multi-directional deformation.

Our echo tracking system had sufficient accuracy to detect bone surface deformation and could monitor the viscoelasticity of bone. Although further investigations will be necessary before this method can be applied to in vivo measurement, our echo tracking method might have a considerable potential for noninvasive measurement of the viscoelasticity and plasticity of bone.

Acknowledgement

References

[1] Hung CT, Allen FD, Pollack SR, Brighton CT. Intracellular Ca^{2+} stores and extracellular Ca^{2+} are required in the real-time Ca^{2+} response of bone cells experiencing fluid flow. J Biomech 1996;29(11):1411–7.

[2] Johnson DL, McAllister TN, Frangos JA, Frangos JA. Fluid flow stimulates rapid and continuous release of nitric oxide in osteoblasts. Am J Phys 1996;271(1Pt1):E205–8.

[3] Reich KM, Frangos JA. Effect of flow on prostaglandin E2 and inositol trisphosphate levels in osteoblasts. Am J Phys 1991;261(3Pt1):C428–32.

[4] Fritton SP, Rubin CT, in: Cowin SC (Ed.), In Vivo Measurement of Bone Deformations Using Strain Gauges. Bone Mechanics Hand Book 8-1, 2nd ed.

[5] Jernberger A. Measurement of stability of tibial fractures. A mechanical method. Acta Orthop Scand 1970;135(Suppl):1–88.

[6] Gail PP, Brian LD, Amy CC, Sudan EDA. An extensometer for global measurement of bone strain suitable for use in vivo in humans. J Biomech 2001;34(3):385–91.

[7] Burr DB, Milgrom C, Fyhrie D, Furwood M, Nyska M, Finestone A, Hoshaw S, Saiag E, Simkin A. In vivo measurements of human tibial strains during vigorous activity. Bone 1996;18(5):405–10.

[8] Lanyon LE, Hampson WGJ, Goodship AE, Shah JS. Bone deformation recorded in vivo from strain gauges attached to the human tibial shaft. Acta Orthop Scand 1975;46:256–68.

[9] Hokanson DE, Mozersky DJ, Sumner DS, Strandness DEJ. A phase-locked echo tracking system for recording arterial diameter changes in vivo. J Appl Physiol 1972;32(5):728–33.

[10] Harada A, Okada T, Niki K, Chang D, Sugawara M. On-line noninvasive one-point measurements of pulse wave velocity. Heart Vessels 2002;17:61–8.

[11] Greenspan M. Tables of the speed of sound in water. J Acoust Soc Am 1959;31(1):75–6.

[12] Laugier P, Padilla F, Camus E, Chaffaï S, Chappard C, Peyrin F, Talmant M, Berger G. Quantitative ultrasound for bone status assessment. IEEE Ultrason Symp. 2000:1341–50.

[13] Sievanen H, Cheng S, Ollikainen S, Uusi-Rasi K. Ultrasound velocity and cortical bone characteristics in vivo. Osteoporos Int 2001;12(5):399–405.

[14] Cortet B, Boutry N, Dubois P, Legroux-Gerot I, Cotten A, Marchandise X. Does quantitative ultrasound of bone reflect more bone mineral density than bone microarchitecture? Calcif Tissue Int 2004;74(1):60–7.

[15] Moorcroft CI, Ogrodnik PJ, Thomas PBM, Wade RH. Mechanical properties of callus in human tibial fractures: a preliminary investigation. Clin Biomech 2001;16:776–82.

[16] Ohnishi I, Nakamura K, Okazaki H, Sato W, Kurokawa T. Evaluation of the fracture site mechanical properties in vivo by monitoring the motion of a dynamic pin clamp during simulated walking. Clin Biomech 2002;17(9/10):687–97.

Nonlinear Finite Element Model Predicts Vertebral Bone Strength and Fracture Site

Kazuhiro Imai, MD, PhD, Isao Ohnishi, MD, PhD, Masahiko Bessho, MD, and Kozo Nakamura, MD, PhD

Study Design. A study on computed tomography (CT)-based finite element (FE) method that predicts vertebral strength and fracture site using human cadaveric specimens.

Objective. To evaluate the accuracy of the nonlinear FE method by comparing the predicted data with those of mechanical testing.

Summary of Background Data. FE methods may predict vertebral strength and fracture site but the prediction has been difficult because of a complex geometry, elastoplasticity, and thin cortical shell of the vertebra.

Methods. FE models of the 12 thoracolumbar vertebral specimens were constructed. Nonlinear FE analyses were performed, and the yield load, the fracture load, the sites where elements failed, and the distribution of minimum principal strain were evaluated. A quasi-static uniaxial compression test for the same specimens was conducted to verify these analyses.

Results. The yield loads, fracture loads, minimum principal strains, and fracture sites of the FE prediction significantly correlated with those measured.

Conclusions. Nonlinear FE model predicted vertebral strength and fracture site accurately.

Key words: vertebral fracture, osteoporosis, fracture strength prediction, nonlinear finite element analysis, fracture site. **Spine 2006;31:1789–1794**

Most vertebral fractures among the elderly occur because of their skeletal fragility due to osteoporosis. To assess the risk of vertebral fracture and its prevention, it is essential to predict vertebral bone strength. Clinically, measurement of bone mineral density by quantitative computed tomography (QCT) and dual energy radiograph absorptiometry (DXA) have been used to predict vertebral strength. However, the correlations between vertebral strength and bone mineral density measured by QCT are reported to be 0.37 to 0.72[1–5] and those with DXA are reported to be 0.51 to 0.80.[4–7] Therefore, such methods only explain 40% to 80% of vertebral strength.

Finite element (FE) models based on data from QCT may predict vertebral strength more accurately because they assess geometry, architecture, and heterogeneous mechanical properties of the bone. CT-based FE models are known to be able to make accurate predictions on fracture loads for femur.[8–12] For vertebra, there have been several attempts to predict fracture strength, and the correlations between compressive vertebral strength and predicted strength were reported to be high (r = 0.89–0.95).[13–16] However, the slopes of the regression line between the measured fracture loads and the predicted were much less than 1.0 (0.569–0.86), and no quantitative prediction could have been made with dependable accuracy. Furthermore, previous models did not compare the fracture sites within a whole vertebra. For clinical application, it is essential for a simulation method to be able to predict both vertebral strength and fracture sites because these are the requisite predictors of a vertebral fracture.

Prediction of vertebral fracture has been difficult because of complex geometry, elastoplasticity, and thin cortical shell of the vertebra. The vertebra has elaborate architecture and geometry with curved surfaces, which cannot be realistically modeled with eight-noded hexahedron elements. Previous mechanical tests showed that there was a difference between tensile and compressive behavior of the bone.[17–19] The compressive behavior showed nonlinear behavior. Therefore, a nonlinear FE model should be used to predict the clinical fracture load.

The cortical shell of the vertebra is estimated to be thin with a thickness of less than 0.5 mm.[20–22] On the other hand, the resolution of a clinically available CT scanner is very low with a pixel spacing larger than 0.25 mm. With the currently available CT resolution, a thin cortical shell cannot be precisely modeled. The thickness tends to be overestimated and its density to be underestimated.[23,24] Therefore, it would be necessary to construct a thinner part of the cortical shell from data that is independent of QCT data.

The purpose of this study was to establish a nonlinear FE model that predicted the vertebral strength and the fracture sites, and then to evaluate the accuracy of our FE model by performing mechanical testing with human cadaveric specimens.

■ Materials and Methods

Twelve thoracolumbar (T11, T12, and L1) vertebrae with no skeletal pathologies were collected within 24 hours of death from 4 males (31, 55, 67, and 83 years old). Causes of death for the four donors were myelodysplastic syndrome, pneumonia,

adult T-cell leukemia, and bladder cancer, respectively. All of the specimens were obtained at University of Tokyo Hospital with the approval of our ethics committee and with informed consent. They were stored at −70 C after each step in our protocol. The vertebrae were disarticulated, and the discs were excised. Then the posterior elements of each vertebra were removed by cutting through the pedicles.

The vertebrae were immersed in water and axial CT images with a slice thickness of 1 mm and pixel width of 0.351 mm were obtained using Lemage SX/E (GE Yokokawa Medical System, Tokyo, Japan) with a calibration phantom containing hydroxyapatite rods.

Nonlinear FE Analysis. The CT data were transferred to a workstation (Endeavor Pro-1000, Epson Direct Co., Nagano, Japan). The three-dimensional FE models were constructed from the CT data using MECHANICAL FINDER software (Mitsubishi Space Software Co., Tokyo, Japan). Trabecular bone was simulated using 2-mm linear tetrahedral elements, and the outer surface of the cortical shell was modeled using 2-mm triangular-plates (Figure 1). The thickness of the cortical shell was set as 0.4 mm based on the previous papers.[20–22] On average, there were 41,133 and 3,191 tetrahedron elements and triangular-plates, respectively.

To allow for bone heterogeneity, the mechanical properties of each element were computed from the Hounsfield unit value. Ash density of each voxel was determined from the linear regression equation created by these values of the calibration phantom. Ash density of each element was set as the average ash density of the voxels contained in one element. Young's modulus and yield stress of each tetrahedron element were calculated from the equations proposed by Keyak et al.[10] Young's modulus of human vertebra cancellous tissue was reported as 3.8 to 13.4 GPa[25–28]; Young's modulus of each triangular-plate was set as 10 GPa. Poisson's ratio of each element was set as 0.4, which was used in the previous papers.[10,29]

A uniaxial compressive load with uniform distribution was applied on the upper surface of the vertebra and all the elements and all the nodes of the lower surface were completely restrained. The models were analyzed using MECHANICAL FINDER. A nonlinear FE analysis by the Newton-Raphson method was used. To allow for the nonlinear phase, mechanical properties of the elements were assumed to be bilinear elastoplastic, and the isotropic hardening modulus was set as 0.05, which is generally used in the analysis of concrete materials.

Each element was assumed to yield when its Drucker-Prager equivalent stress reached the element yield stress. Failure was defined as occurring when the minimum principal strain of an element was less than −10,000 microstrain. Vertebral yield was defined as being when at least one element yielded, and vertebral fracture was defined as being when at least one element failed. The yield load, the fracture load, the sites where elements failed, and the distribution of minimum principal strain were analyzed.

Quasi-Static Uniaxial Compressive Load Testing. To verify the simulations, a quasi-static uniaxial compression test of each vertebra was conducted. Load, cross-head displacement, and principal strain at the vertebral surface were measured. To restrain the specimens for load testing, both upper and lower surfaces of the vertebrae were embedded in dental resin (Ostron; GC Dental Products Co., Aichi, Japan) so that the two surfaces were exactly parallel. Then the embedded specimens were placed on a mechanical testing machine (TENSILON UTM-2.5T; Orientec, Tokyo, Japan) and were compressed at a cross-head displacement rate of 0.5 mm per minute. A compression plate with a ball joint was used to apply a uniform load onto the upper surface of the specimen. The applied load was measured by a load cell (T-CLB-5-F-SR; T. S. Engineering, Kanagawa, Japan). The load and the cross-head displacement were recorded using MacLab/4 (AD Instruments, Castle Hill, NSW, Australia) at a sampling rate of 2 Hz. For 9 of the 12 vertebrae, one of the four rosette strain gauges (SKF-22358; Kyowa Electronic, Tokyo, Japan) was attached to each of anterior, left, right, and posterior surfaces of the vertebra. The strain readings were recorded at a sampling rate of 0.5 Hz and stored by a data logger (U-CAM-20PC-1; Kyowa Electronic); then principal strain was calculated at each of the attachment sites. The measured yield load was defined as the load that reached the end of the plateau of the constant load increment rate, which corresponded with the end of the linear phase on the load displacement curve. The measured fracture load was defined as the ultimate load achieved (Figure 2). To determine the actual fracture sites, anteroposterior and lateral soft radiograph pictures (Softex, Kanagawa, Japan) and micro-CT (MCT-CB100MF: Hitachi Medico Technology Corp., Tokyo, Japan) images scanned with 70 kV, 100 μA, and a voxel size of 107 μm were obtained after the mechanical testing. The micro-CT images were processed and reconstructed to obtain the images at the midsagittal cross section and at the midfrontal cross section. The sites and the types of experimental fractures were judged from the soft radiograph pictures and the reconstructed micro-CT images.

A three-dimensional surface acquisition system using an image encoder (VOXELAN; Hamano Engineering, Kanagawa, Japan) was used to identify the gauge attachment sites on the shell elements by matching the three-dimensional surface image with the FE model. All three images, i.e., the three-dimensional mesh model, the two-dimensional digitized image, and the three-dimensional surface image, were matched and the strain gauge attachment sites were then identified (Figure 3). The minimum principal strain was calculated with an applied load of 1,000 N, under which all specimens were in the elastic phase.

Pearson's correlation analysis was used to evaluate correlations between the predicted and the measured fracture loads, as well as between the predicted and the measured minimum principal strains.
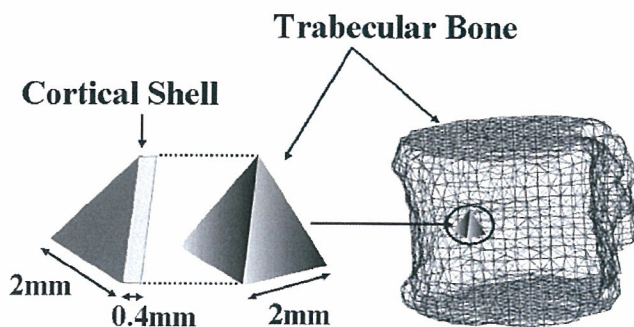

Figure 1. A finite element model of a whole vertebral body. Trabecular bone was simulated using 2-mm tetrahedron elements, and cortical shell was modeled by 2-mm triangular-plates with a thickness of 0.4 mm. This model consisted of 12,938 nodes with 70,022 tetrahedron elements and 3,586 triangular-plates.
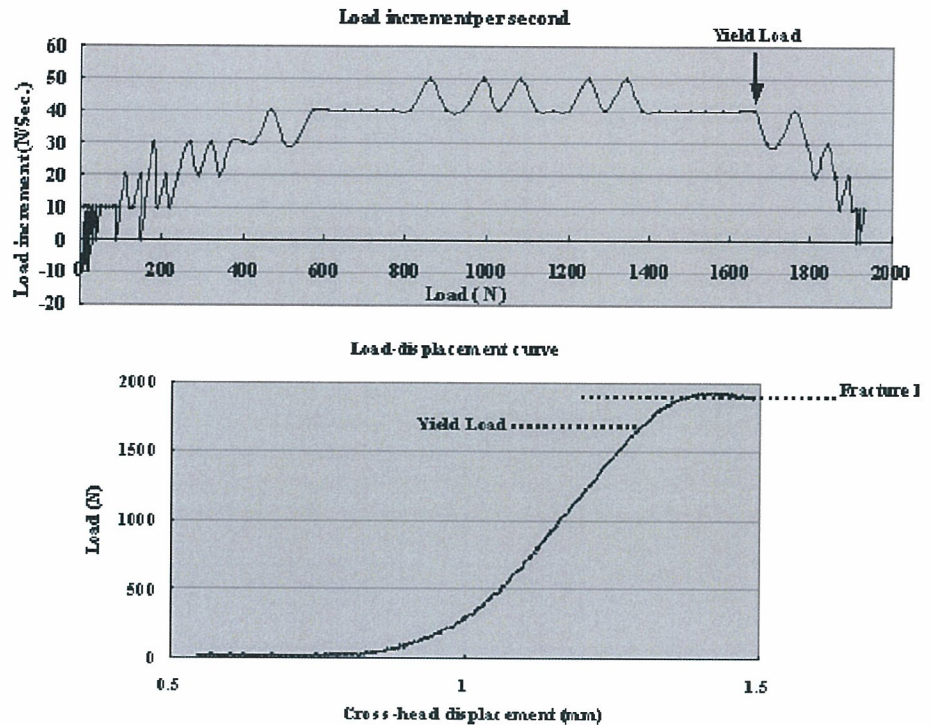
Figure 2. The definition of the experimental yield load and the fracture load. The experimentally measured yield load was defined as the load that reached the end of the constant load increment rate. The measured fracture load was defined as the ultimate load achieved.

■ Results

There was a significant linear correlation between the yield loads predicted by the FE analysis and those of the measured (r = 0.949, P < 0.0001) (Figure 4). The correlation between the FE predicted fracture loads and the measured was even stronger (r = 0.978, P < 0.0001), and the slope of the regression line was 0.8807 (Figure 5). There was also a significant linear correlation between the FE predicted minimum principal strain and the measured (r = 0.838, P < 0.0001) (Figure 6).

There were two types of experimental fractures. Obvious fracture lines were recognized in six vertebrae. There were no obvious fracture lines in the other six, but they had apparent residual deformities after the mechan-

ical testing. The anterior part of the vertebra was compressed in three of the six. The other two sustained middle part compression and in one there was compression of the entire vertebra.

The experimental fracture line in the specimen was found to pass through a region of the failed elements on the simulation model (Figure 7). In addition, the FE analysis of the minimum principal strain at the midsagittal section disclosed that the area with a large absolute value of this predicted minimum principal strain agreed well with the experimental fracture site and that it visualized the fractured area.

In the specimens with anterior compression, marked radiolucency was recognized at the anterior part of the
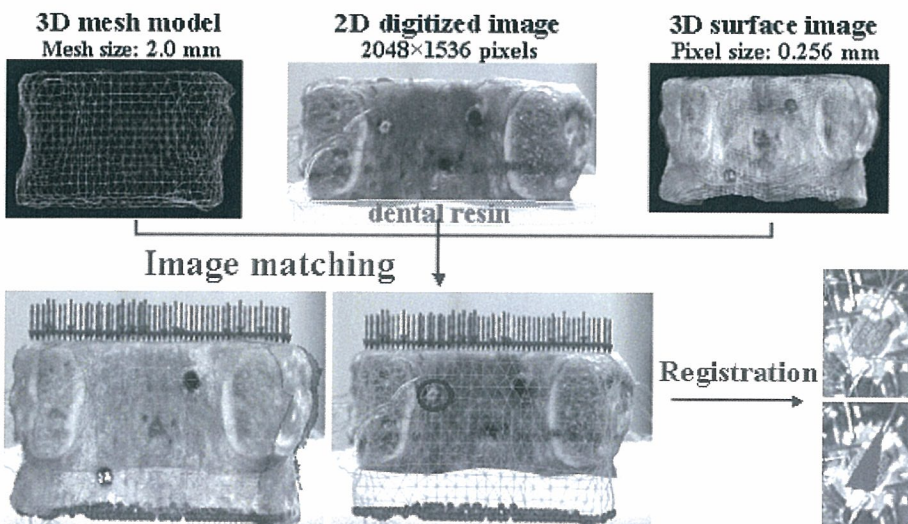

Figure 3. A three-dimensional surface acquisition system was employed to identify the gauge attachment sites by matching the three-dimensional surface image with the FE model. The three-dimensional mesh model, the two-dimensional digitized image, and the three-dimensional surface image, were matched and the strain gauge attachment sites were then identified.
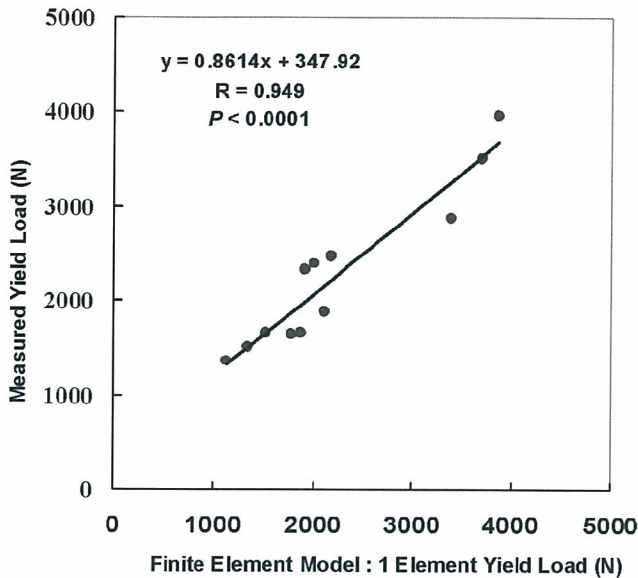
Figure 4. The experimentally measured yield loads versus the yield loads predicted by the finite element (FE) analysis. They were significantly correlated.

Figure 6. The values of measured minimum principal strain versus those of minimum principal strain predicted by the FE model. Significant correlation was also obtained.

vertebra, where the trabecular pattern was observed to be very coarse (Figure 8). The FE analysis showed that the failed elements appeared at the same anterior part as the area with coarse trabeculae. Likewise, the area with large absolute value of the minimum principal strain localized at the anterior part, which agreed with the area of the experimental compression fracture.

■ Discussion

The correlations between the measured values of fracture strength and the predicted values with the FE model were very good (r = 0.978) and better than the previous FE studies (r = 0.89–0.95). The characteristics of the FE

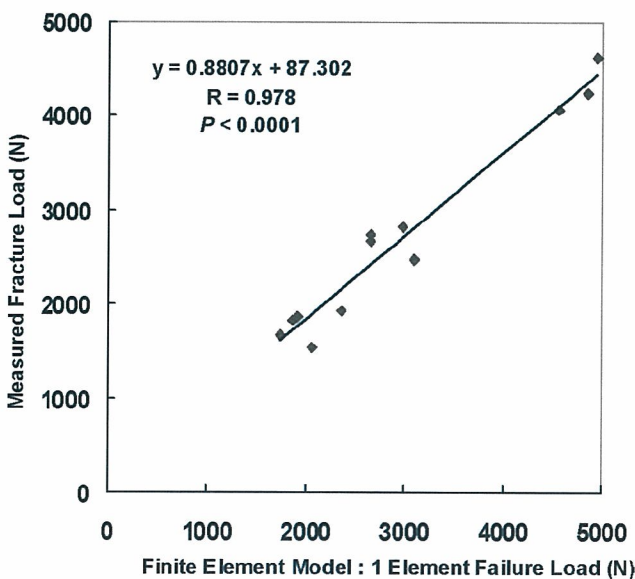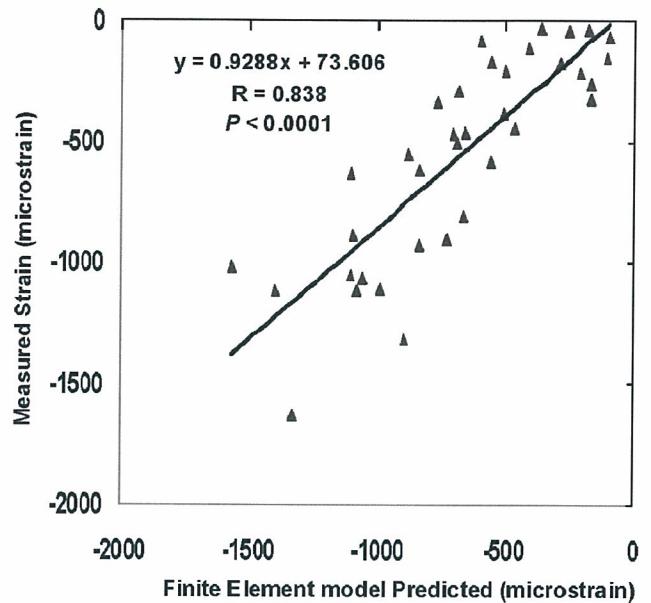

Figure 5. The measured fracture loads versus the fracture loads predicted by the FE model. The correlation was much better with a slope of 0.8807.

model in this study were as follows: adoption of tetrahedron elements to precisely model surface curvatures of the entire vertebra, utilization of nonlinear analysis to match the elastoplasticity of the vertebra in compression, construction of cortical shells on the surface of the model, and adoption of Drucker-Prager equivalent stress instead of von Mises stress as a criterion of an element yield. Which of these factors contributed most to the results was not determined in this study because we did not separate these characteristics to analyze each factor's contribution. Clarification of this feature will be one of our targets for the next study.

With tetrahedron elements, it was possible to create a more proximate, realistic and smooth surface contour than with hexahedral elements, which could possibly avoid any artificial stress raisers.

With the currently available CT resolution, strength of the cortical shell tended to be underestimated. In CT-based FE models, density of this shell has been underestimated because it is dependent on its Hounsfield unit value. It has been reported that in previous experiments thin cortical shell of the vertebrae contributed approximately 10% to the overall vertebral strength in healthy individuals and the contribution of the cortical shell was estimated to be significantly larger in osteoporotic individuals.[2,30] Thus, the importance of the strength of the cortical shell should be taken into consideration in predicting the fracture load of osteoporotic individuals.

Overaker *et al* set the thickness of the anterior cortex as 0.6 mm and that of the posterior as 0.4 mm; they set the cortical Young's modulus as 5, 6, 7 GPa. They concluded that Young's modulus of 7 GPa precisely correlated with the experimental result.[29] Liebschner *et al* set the thickness as 0.35 mm and Young's modulus as 0.475 GPa.[15] We
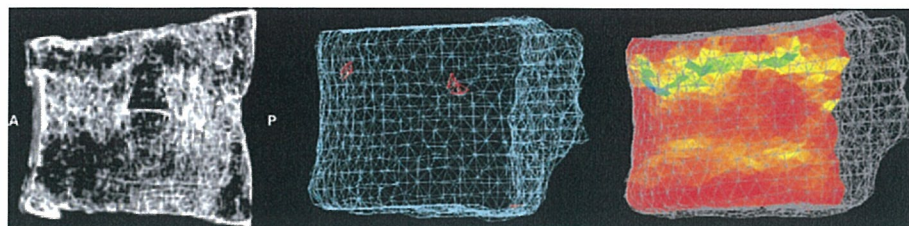
Figure 7. The reconstructed micro-CT images (A, anterior; P, posterior), the failed elements, and the minimum principal strain distribution at the mid-section analyzed by the FE model. The failed elements appeared right on the actual fracture line. The minimum principal strain distribution agreed well with the experimental fracture line.

constructed a cortical shell with a thickness of 0.4 mm and Young's modulus of 10 GPa. The cortical area with a thickness of more than 0.4 mm was modeled with both the shell and the tetrahedron element adjacent to the shell.

Young's modulus of human cortical bone has been reported to be 15 GPa,[31] 19.9 GPa (dynamic), and 16.2 GPa (static).[32] Young's modulus of human vertebra cancellous tissue was reported as 3.8 to 13.4 GPa,[25–28] but few data of cortical shell have been available. Thus, it was necessary to set our own value. Young's modulus of the cortical shell obtained from the QCT data were 7 GPa. QCT underestimated the cortical shell density, so the actual density was estimated to be higher than that derived from QCT. Therefore, we set Young's modulus as 10 GPa, and then the values of the minimum principal strain were accurately predicted with a correlation coefficient of 0.838 and a slope of the regression line of 0.9288.

In previous studies, von Mises equivalent stress has been used as the criterion of yield.[8,10,13] For ductile materials such as metals, von Mises criterion would be effective, but for bones it seems more appropriate to use Drucker-Prager equivalent stress. The yield strain of human vertebral trabecular bone was reported −7,000 to −10,000 microstrain.[17,18] Therefore, we adopted minimum strain of −10,000 microstrain as a criterion for element collapse.

Some previous reports described the mechanical properties of human bone. We tested three theories: Carter and Hayes' property,[33,34] Keller's,[35] and Keyak's.[10] With Carter and Hayes' property, the predicted fracture loads were about 60% and using Keller's, the predicted fracture loads were about 120% of those of the experiment. Accurate prediction could be made with Keyak's, although further investigations will be necessary to obtain the actual mechanical properties of human vertebra.

In this investigation, prediction of the ultimate load was more accurate than that of the yield load. One pos-

sibility was that determination of the experimental yield load was not appropriate. The ultimate load was clearly determined, but the yield load was objectively determined from load *versus* displacement curves by calculating the load increment rate (Figure 2).

There were two types of vertebral fracture: one showed fracture line and the other showed no fracture lines but had apparent residual deformities. Both fracture types could be predicted. Fracture location was most accurately predicted by the distribution of very low levels of the minimum principal strain. Therefore, we speculated that fracture was initiated at the sites of failed elements and propagated along with the area with very low minimum principal strain.

The prediction was made under a very simple loading condition with quasi-static uniaxial vertical loading. The condition was the simplest, but it minimized experimental error, which might have occurred to some degree with complicated loading conditions. Arbitrary load magnitude or direction can be set for the same simulation model. So it is possible to analyze strength or fracture site of vertebrae for loading conditions that actually cause fractures, although it would be very hard to create these fractures under an experimental condition. To predict in vivo behavior of spinal bones is another target for our next study.

To verify our model, we evaluated three factors: fracture strength, fracture site, and strain on the surface of the vertebrae. Prediction of only fracture strength would not be adequate to evaluate the accuracy of FE analysis. Predicted fracture sites should also be matched with those of the experiment, and the process by which deformation of the vertebrae proceeds should be simulated. To attain this, we used strain gauges to measure surface strain throughout the loading process. This has not been done in previous studies investigating the accuracy of a simulation model.

The limitation is the cortical shell was treated as a homogeneous material because the pixel spacing with

Figure 8. Radiogram after the mechanical testing, showing sparse trabecula in the anterior part of the vertebral body. The failed elements agreed well with the site of the experimental fracture. The minimum principal strain distribution also agreed well with the area of the experimental fracture.
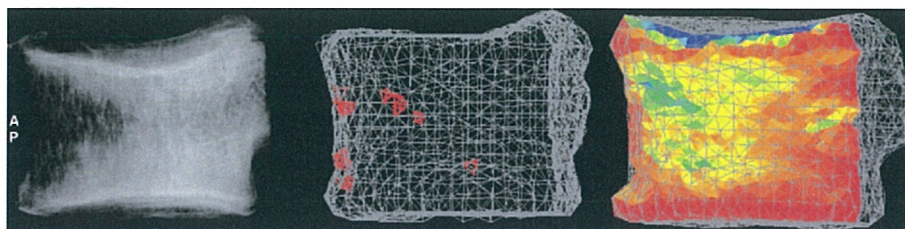
CT is too large to model the thin cortical shell. If a CT with improved resolution becomes available, it would make it possible to model the cortical shell with heterogeneous properties, thus enabling creation of a more realistic model.

There is another limitation. The posterior portion of the vertebra was excised in this study. A three-dimensional surface acquisition system using an image encoder was used to identify the gauge attachment sites on the shell elements. With the posterior portion of the vertebra such as lamina or spinous process, obtaining three-dimensional surface image of the posterior part of the vertebral body should be interfered. It was one of the reasons why the posterior portion of the vertebra was excised. Clinically, most of the vertebral fractures occur at the vertebral body. However, the posterior portion of the vertebra might share some ratio of axial loading. Therefore, loading environment in the in vivo situation may be different from that in this study. To predict in vivo behavior of spinal bones, the posterior portion of the vertebra must be included.

The cadaveric specimens were all extracted from males, whose bone quality might be somewhat different from that of females. To use this model as a diagnostic tool for osteoporosis, it would have been better to use specimens from both males and females. Validation of accurate prediction by the FE model in an experiment using female cadaveric specimens will be another target of our future study. Furthermore, true efficacy of this method will be validated after a large-scale cohort study investigating the association between the predicted fracture loads in the study groups and the occurrence rates of actual fracture in the same groups. It is expected that this method will be valuable in estimating fracture risk of vertebrae in osteoporotic individuals.

■ Key Points

- Vertebral strength and fracture site were accurately predicted using nonlinear finite element model.
- The minimum principal strain at the vertebral surface was also predicted.
- The experimental fracture sites corresponded with the sites where the elements were predicted to fail.

References

1. Mosekilde L, Bentzen SM, Ortoft G, et al. The predictive value of quantitative computed tomography for vertebral body compressive strength and ash density. *Bone* 1989;10:465–70.
2. McBroom RJ, Hayes WC, Edwards WT, et al. Prediction of vertebral body compressive fracture using quantitative computed tomography. *J Bone Joint Surg Am* 1985;67:1206–14.
3. Brinckmann P, Biggemann M, Hilweg D, et al. Prediction of the compressive strength of human lumbar vertebrae. *Clin Biomech* 1989;4(suppl):1–27.
4. Edmondston SJ, Singer KP, Day RE, et al. In-vitro relationships between vertebral body density, size and compressive strength in the elderly thoracolumbar spine. *Clin Biomech* 1994;9:180–6.
5. Cheng XG, Nicholson PH, Boonen S, et al. Prediction of vertebral strength in vitro by spinal bone densitometry and calcaneal ultrasound. *J Bone Miner Res* 1997;12:721–8.
6. Myers BS, Arbogast KB, Lobaugh B, et al. Improved assessment of lumbar vertebral body strength using supine lateral dual-energy x-ray absorptiometry. *J Bone Miner Res* 1994;9:687–93.
7. Bjarnason K, Hassager C, Svendsen OL, et al. Anteroposterior and lateral spinal DXA for the assessment of vertebral body strength: comparison with hip and forearm measurement. *Osteoporos Int* 1996;6:37–42.
8. Lotz JC, Cheal EJ, Hayes WC. Fracture prediction for the proximal femur using finite element models: I. Linear analysis. *J Biomech Eng* 1991;113:353–60.
9. Lotz JC, Cheal EJ, Hayes WC. Fracture prediction for the proximal femur using finite element models: II. Nonlinear analysis. *J Biomech Eng* 1991;113:361–5.
10. Keyak JH, Rossi SA, Jones KA, et al. Prediction of femoral fracture load using automated finite element modeling. *J Biomech* 1998;31:125–33.
11. Keyak JH. Improved prediction of proximal femoral fracture load using nonlinear finite element models. *Med Eng Phys* 2001;23:165–73.
12. Cody DD, Gross GJ, Hou FJ, et al. Femoral strength is better predicted by finite element models than QCT and DXA. *J Biomech* 1999;32:1013–20.
13. Silva MJ, Keaveny TM, Hayes WC. Computed tomography-based finite element analysis predicts failure loads and fracture patterns for vertebral sections. *J Orthop Res* 1998;16:300–8.
14. Martin H, Werner J, Andresen R, et al. Noninvasive assessment of stiffness and failure load of human vertebrae from CT-data. *Biomed Tech* 1998;43:82–8.
15. Liebschner MA, Kopperdahl DL, Rosenberg WS, et al. Finite element modeling of the human thoracolumbar spine. *Spine* 2003;28:559–65.
16. Crawford RP, Cann CE, Keaveny TM. Finite element models predict in vitro vertebral body compressive strength better than quantitative computed tomography. *Bone* 2003;33:744–50.
17. Keaveny TM, Wachtel EF, Ford CM, et al. Differences between the tensile and compressive strengths of bovine tibial trabecular bone depend on modulus. *J Biomech* 1994;27:1137–46.
18. Kopperdahl DL, Keaveny TM. Yield strain behavior of trabecular bone. *J Biomech* 1998;31:601–8.
19. Morgan EF, Keaveny TM. Dependence of yield strain of human trabecular bone on anatomic site. *J Biomech* 2001;34:569–77.
20. Silva MJ, Wang C, Keaveny TM, et al. Direct and computed tomography thickness measurements of the human, lumbar vertebral shell and endplate. *Bone* 1994;15:409–14.
21. Vesterby A, Mosekilde L, Gundersen HJ, et al. Biologically meaningful determinants of the in vitro strength of lumbar vertebrae. *Bone* 1991;12:219–24.
22. Mosekilde L. Vertebral structure and strength in vivo and in vitro. *Calcif Tissue Int* 1993;53(suppl):121–6.
23. Dougherty G, Newman D. Measurement of thickness and density of thin structures by computed tomography: a simulation study. *Med Phys* 1999;26:1341–8.
24. Prevrhal S, Engelke K, Kalender WA. Accuracy limits for the determination of cortical width and density: the influence of object size and CT imaging parameters. *Phys Med Biol* 1999;44:751–64.
25. Jensen KS, Mosekilde L. A model of vertebral trabecular bone architecture and its mechanical properties. *Bone* 1990;11:417–23.
26. Rho JY, Tsui TY, Pharr GM. Elastic properties of human cortical and trabecular lamellar bone measured by nanoindentation. *Biomaterials* 1997;18:1325–30.
27. Hou FJ, Lang SM, Hoshaw SJ, et al. Human vertebral body apparent and hard tissue stiffness. *J Biomech* 1998;31:1009–15.
28. Ladd AJ, Kinney JH, Haupt DL, et al. Finite-element modeling of trabecular bone: comparison with mechanical testing and determination of tissue modulus. *J Orthop Res* 1998;16:622–8.
29. Overaker DW, Langrana NA, Cuitino AM. Finite element analysis of vertebral body mechanics with a nonlinear microstructural model for the trabecular core. *J Biomech Eng* 1999;121:542–50.
30. Faulkner KG, Cann CE, Hasegawa BH. Effect of bone distribution on vertebral strength: assessment with patient-specific nonlinear finite element analysis. *Radiology* 1991;179:669–74.
31. Choi K, Kuhn JL, Ciarelli MJ, et al. The elastic moduli of human subchondral, trabecular, and cortical bone tissue and the size-dependency of cortical bone modulus. *J Biomech* 1990;23:1103–13.
32. Katsamanis F, Raftopoulos DD. Determination of mechanical properties of human femoral cortical bone by the Hopkinson bar stress technique. *J Biomech* 1990;23:1173–84.
33. Carter DR, Hayes WC. Bone compressive strength: the influence of density and strain rate. *Science* 1976;194:1174–6.
34. Carter DR, Hayes WC. The compressive behavior of bone as a two-phase porous structure. *J Bone Joint Surg Am* 1977;59:954–62.
35. Keller TS. Predicting the compressive mechanical behavior of bone. *J Biomech* 1994;27:1159–68.